

We are IntechOpen, the world's leading publisher of Open Access books Built by scientists, for scientists

6,900

Open access books available

186,000

International authors and editors

200M

Downloads

Our authors are among the

154

Countries delivered to

TOP 1%

most cited scientists

12.2%

Contributors from top 500 universities



WEB OF SCIENCE™

Selection of our books indexed in the Book Citation Index
in Web of Science™ Core Collection (BKCI)

Interested in publishing with us?
Contact book.department@intechopen.com

Numbers displayed above are based on latest data collected.
For more information visit www.intechopen.com



Multi-Elliptical Geometry of Scatterers in Modeling Propagation Effect at Receiver

Jan M. Kelner and Cezary Ziólkowski

Additional information is available at the end of the chapter

<http://dx.doi.org/10.5772/intechopen.75142>

Abstract

In the proposed chapter, the authors present a geometric-statistical propagation model that defines three groups of received signal components, i.e., direct path, delayed scattering, and local scattering components. The multi-elliptical propagation model, which represents the geometry of scatterer locations, is the basis for determining the delayed components. For the generation of the local components, a statistical distribution is used. The basis for this model is a power angular spectrum (PAS) of the received signal, which is closely related to a type of propagation environment and transmitter-receiver spatial positions. Therefore, we have an opportunity to evaluate the influence of the environment type and an object motion direction on the basic characteristics such as envelope distribution, PAS, autocorrelation function, and spectral power density. The multi-elliptical model considers the propagation phenomena occurring in the azimuth plane. In the chapter, we will also show the 3D extension of modeling effects of propagation phenomena.

Keywords: radio wave propagation, propagation modeling, channel modeling, geometric-based model, multi-elliptical model, multi-ellipsoidal model, scattering, angular power spectrum, angle spread, angular dispersion, directional antenna pattern, power delay profile, simulation

1. Introduction

A development of information and communication systems is characterized by a dynamic increase in demand for the provision of telecommunication services with the participation of wireless networks. A limitation of frequency resources forces the search for new methods of effective spectrum management. One of the solutions to this problem is spatial multiplexing of network access, which minimizes a field strength and increases access area of the network.

This solution is based on the use of an active phased array antenna (APAA) or massive APAA and is applicable to emerging fifth generation (5G) systems. In these systems, the multiple use of the same frequency bands is qualified by no interference between individual wireless links. Fulfillment of this condition has a large impact on received signals, properties of which significantly depend on a direction of reaching an electromagnetic wave to a reception point. This means that the prediction, modeling, and evaluation of statistical properties of the receipt direction play an important role in assessing internal and external conditions of a compatible operation of wireless networks. This fact justifies the purposefulness of topics presented in this chapter.

The goal of the chapter is to describe the methods for determining the statistical properties of the signal reception angle and its parameters. Particular attention is given to an impact analysis of directional antenna parameters on the statistical parameters and characteristics that describe dispersion of reception angle. The main purpose of this chapter is based on geometric propagation models in which scatterer locations are determined by multi-elliptical curves or multi-ellipsoidal surfaces.

Due to a method of determining the statistical characteristics of a reception angle, propagation models can be divided in accordance with the diagram presented in **Figure 1**.

Measurement data and standard distributions such as the Gaussian, Laplacian, logistic, and von Mises distribution are the basis for empirical models that directly describe a probability density function (PDF) of angle of arrival (AOA) [1–3]. In this case, developing a model consists in such adjustment of distribution parameters that will ensure minimization of approximation error to the measurement data. For the first three models mentioned above, the approximation problem comes down to determining the normalizing constant and parameters that define these distributions [1]. For the von Mises distribution [4], the approximation consists in adjusting a single parameter, which simplifies the procedure of creating the statistical model of the reception angle distribution [1].

In practice, complex empirical models are used. They use standard distributions to describe the statistical properties of individual angular clusters. Examples of such models are defined, i.e., by the WINNER projects [5] and 3rd Generation Partnership Project (3GPP) [6, 7]. The

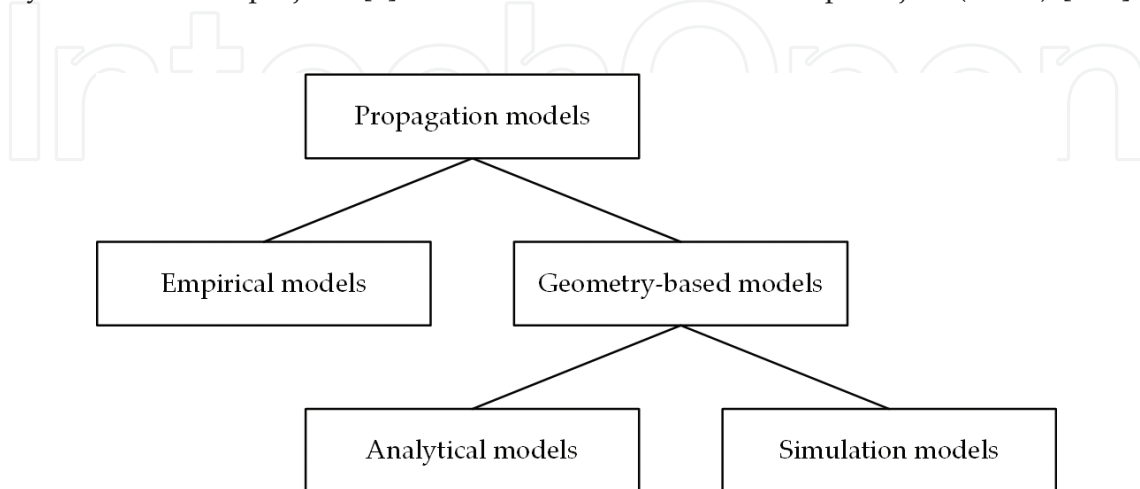


Figure 1. Classification of propagation models due to method of determining statistical properties of reception angle.

main disadvantages of these models are the lack of consideration of antenna pattern influence and distance between a transmitter (Tx) and receiver (Rx).

These disadvantages do not have geometrical models. These models are defined by geometrical structures that determine positions of elements scattering an electromagnetic wave. Knowledge of propagation environment geometry gives the possibility to determine the signal reception directions. This task can be carried out analytically or through simulation research.

The use of geometrical optics is one of the basic methods of determining AOA, which considers the geometric structure of propagation environment. A ray tracing is practical implementation of this propagation modeling method [8–12]. The accuracy of the obtained results depends to a large extent on the accuracy of mapping electrical properties of all elements forming the electromagnetic environment and the number of generated rays. The difficulty of obtaining environmental data and the complexity of simulation procedures are the reason for limited reliability of the results obtained by this method. A concept of propagation paths [13] gives the possibility of simplifying the ray-tracing method. In this case, the analysis comes down to an evaluation of propagation paths in the presence of scattering elements (scatterers) whose position on the plane (two-dimensional (2D) modeling) or in space (three-dimensional (3D) modeling) maps specific geometric structures.

A shape of scatterer occurrence areas, their position relative to the Tx and Rx locations, and a density distribution are the criteria that differentiate individual models. For the 2D areas, geometric structures such as a circle [5, 6, 14–16], ellipse [15, 16], hollow disk [17], and elliptical disk [18] are most commonly used. In the case of 3D, the scatterer areas represent a sphere [19], semi-spheroid [20, 21], clipping semi-spheroid [22], semi-ellipsoid [23], cylinder [24, 25], and complex solid figures, for example, bounded ellipsoid and elliptical cylinder [26] or sphere and ellipsoid [27].

The density of the scatterers is another criterion that differentiates the individual geometric models. The uniform distribution is most widely used to describe spatial concentration of the scattering elements, especially with regard to limited geometrical structures, e.g., [14, 15, 22, 28–30]. For models where the scatterer occurrence area is unrestricted, the normal distribution is used, e.g. [4, 22, 31].

The area geometry and density of the scatterer occurrence give the possibility to determine the approach directions of the propagation paths to the Rx. However, the practical use of the geometric models to assess the statistical properties of the reception angle is largely hampered. This fact results from the lack of a relationship between the geometry of these models and transmission properties of the propagation environment. These properties are described by a channel impulse response and related characteristics such as a power delay profile (PDP) or power delay spectrum (PDS). Nevertheless, in the set of all models, we can distinguish geometrical structures whose parameters are defined by the channel transmission characteristics. Multi-elliptical and multi-ellipsoidal propagation models are these special cases. Consideration of the relationship between the transmission parameters and geometrical structures ensures minimization of the approximation error between measurement data and modeling results.

This chapter is devoted to the evaluation of the statistical properties of the scattering, a reception angle, and the effects of this phenomenon, which has a significant impact on correlational and spectral properties of the received signals. The multi-elliptical and multi-ellipsoidal propagation models are the basis for the analysis presented in the chapter.

2. Environment transmission properties and propagation model geometry

Statistical evaluation of the radio channel transmission properties is based on the energetic measures of the received signals. PDPs and PDSs describe powers and delays of individual components that reach the Rx. An example of PDP, $P(\tau)$, defined by 3GPP [7, Table 7.7.2–2] is shown in **Figure 2**. In this case, the PDP represents non-line-of-sight (NLOS) conditions, urban macro (UMa)-environment type with delay spread, $\sigma_\tau = 363$ ns which is characteristic of the carrier frequency, $f_0 = 2$ GHz.

The PDP graph shows that the received signal is a superposition of component groups that form time clusters with different delays. Measurement results presented in a literature justify the following assumptions:

- Components that undergo single scattering have a dominant energetic significance.
- The probability of the scatterer occurrence seen from the Tx is the same in every direction.
- For each element, the statistical properties of scattering factor module and phase are the same.

Thus, all signal components that arrive at the Rx with the same delay come from the scatterers located on the same ellipsoid. This means that the number of the ellipsoids that represent the scatterer locations is equal to the number of the time clusters. Their foci determine the Tx and Rx positions.

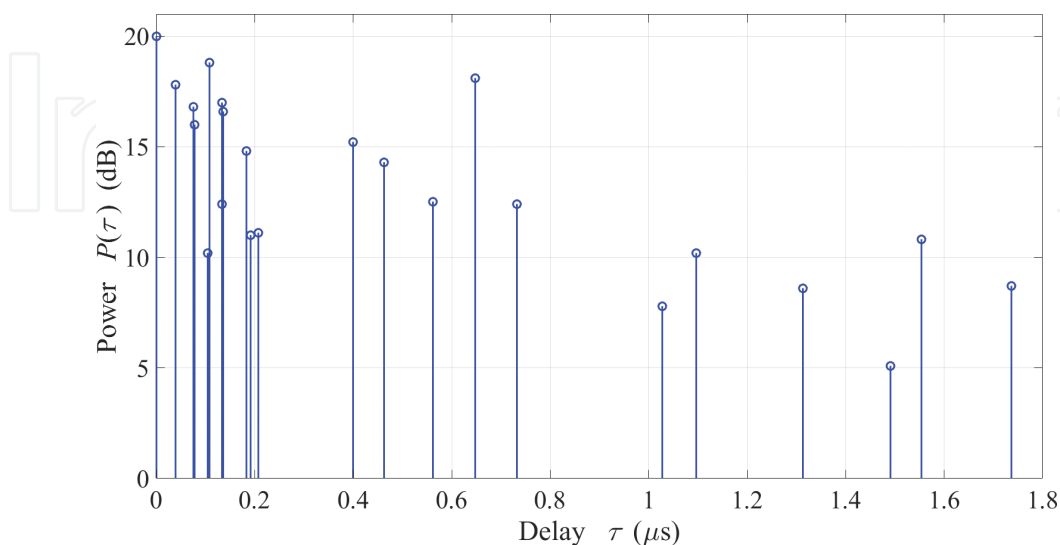


Figure 2. Example of PDP for UMa NLOS 2 GHz environment from 3GPP.

For majority of wireless links, relations between heights of the Tx (h_T)/Rx (h_R) antennas and their distance, D , meet a condition, $h_T, h_R \ll D$. In the case of ground wave propagation, this condition is the basis for reduction of the scattering areas to semi-ellipsoids. The use of the antennas, whose radiation patterns are narrow in the elevation plane, brings the 3D to 2D modeling. For these conditions, the multi-ellipsoidal model is reduced to the multi-elliptical model of scattering areas, as shown in **Figure 3**.

The delays of the individual time clusters, τ_i for $i = 1, 2, \dots, N$, define the parameters of the corresponding semi-ellipsoids. For the i th semi-ellipsoid, we have

$$a_i = \frac{1}{2}(D + c\tau_i), \quad b_i = c_i = \frac{1}{2}\sqrt{c\tau_i(2D + c\tau_i)} \quad (1)$$

where c is the speed of light.

Each time cluster is the superposition of the signal components that reach the Rx from the scatterers located on the respective semi-ellipsoids. The reception directions of these components

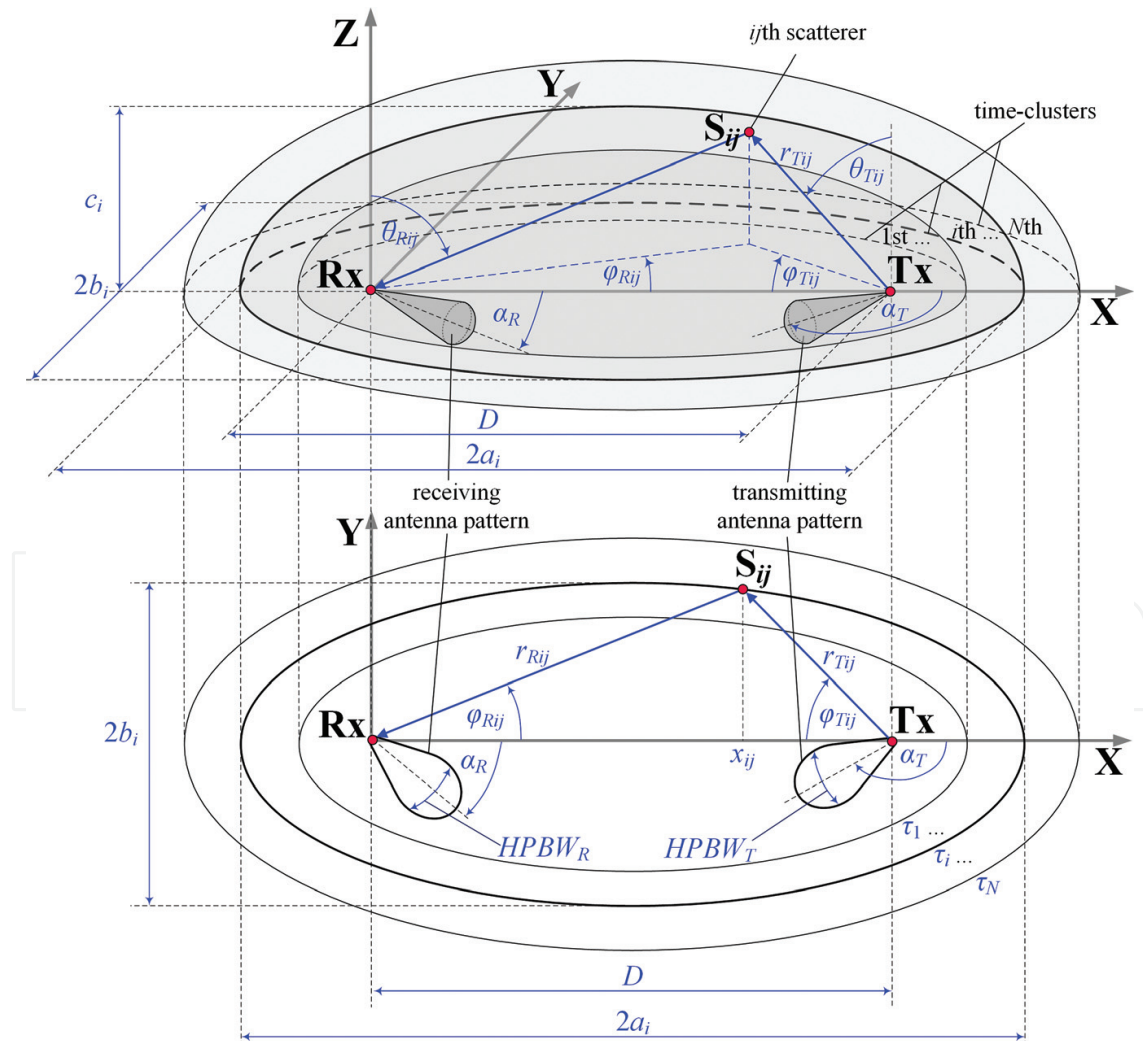


Figure 3. 3D and 2D models of scattering areas.

are determined by the shape of the scatterer occurrence surface. This means that the powers of the individual clusters depend on the propagation path direction to the Rx. Differentiation of the cluster delays is the basis for expressing a power angular spectrum (PAS) as a sum of the component powers reaching the Rx with the delays, $P_R(\theta_R, \varphi_R)$, and the component powers, $P_{R0}(\theta_R, \varphi_R)$, whose delays are of the order of a carrier wave period. The first and second groups of components are called the delayed and local scattering components, respectively.

The delayed components are grouped in the time clusters. Therefore,

$$P_R(\theta_R, \varphi_R) = \sum_{i=1}^N P_{Ri}(\theta_R, \varphi_R) + P_{R0}(\theta_R, \varphi_R) \quad (2)$$

where N is the number of the time clusters (semi-ellipsoids) and $P_{Ri}(\theta_R, \varphi_R)$ means the PAS of the propagation paths that reach the Rx from the i th ellipsoid.

The PAS can be presented as the product of a total power and PDF of AOA [32]. We should also note that $P_{R0}(\theta_R, \varphi_R)$ represents the sum of the powers of the direct path component and the local scattering components. The energy relationship between these components describes the Rice factor, κ . Thus, we can present the PDF of AOA, $f_R(\theta_R, \varphi_R)$, which describes the statistical properties of the signal reception angle, in the following form:

$$\begin{aligned} f_R(\theta_R, \varphi_R) &= f_d(\theta_R, \varphi_R) + f_l(\theta_R, \varphi_R) + f_{dp}(\theta_R, \varphi_R) \\ &= \sum_{i=1}^N \frac{P_i}{P} f_i(\theta_R, \varphi_R) + \frac{\kappa}{1+\kappa} \frac{P_0}{P} f_0(\theta_R, \varphi_R) + \frac{1}{1+\kappa} \frac{P_0}{P} \delta(\theta_R, \varphi_R) \end{aligned} \quad (3)$$

where $f_d(\theta_R, \varphi_R)$, $f_l(\theta_R, \varphi_R)$, and $f_{dp}(\theta_R, \varphi_R)$ represent parts of $f_R(\theta_R, \varphi_R)$ corresponding the delayed scattering components, local scattering components, and direct path component, respectively, P is the total power of the received signal, P_i is the power of the propagation paths reaching the Rx from the i th ellipsoids, $f_i(\theta_R, \varphi_R)$ means PDF of AOA for the i th ellipsoids, P_0 represents the power of the components reaching the Rx with negligible delay, $f_0(\theta_R, \varphi_R)$ is PDF of AOA for the local scattering components, and $\delta(\cdot)$ is the Dirac delta function.

For the delayed components, the multi-ellipsoidal or multi-elliptical structures are the basis for the analytical or simulation determination of individual $f_i(\theta_R, \varphi_R)$, $i = 1, 2, \dots, N$. In the case of the local scattering, a large diversity of receiving antenna surroundings prevents adoption of a determined geometry of the scatterer positions. To adapt the statistical properties of reception angle, the von Mises distribution is used [4].

Construction of the multi-ellipsoidal or multi-elliptical structures based on PDP/PDS ensures adjustment of the reception angle statistical characteristics to the transmission properties of the propagation environment. In that, these models provide a mapping of the impact of these properties on the correlational and spectral characteristics of the received signals.

The correctness of the adopted model is confirmed by comparative analyses with empirical data presented, among others, in [33–36]. From these analyses, it appears that the multi-elliptical model provides the smallest errors of PAS and PDF of AOA approximation to other geometric and empirical models. The correctness of the adopted model is confirmed by comparative analyses with empirical data presented in, e.g., [37].

3. Multi-elliptical propagation model

The use of the antennas with the narrow radiation patterns in the elevation plane limits an environment influence on the received signal properties. Propagation phenomena predominance in the azimuth plane is the premise for reducing the analysis of the reception angle statistical properties to the 2D modeling problem. In this case, the mapping of the propagation phenomena is ensured by the multi-elliptical propagation model. Precursors of this model are Parsons and Bajwa, who presented a multi-elliptical way of modeling the distribution of the propagation paths in [38].

3.1. Analysis of reception angle statistical properties for omni-directional antennas

A PDF of AOA analysis for radio links with omni-directional antennas is based on the 2D geometric structure shown in **Figure 3**. In this case, Eq. (3) shows that determining the PDF of AOA for the delayed components comes down to determining $f_i(\varphi_R)$.

Propagation path lengths, i.e., r_{Tij} and r_{Rij} (see **Figure 3**), which describe the distances $\overline{TxS_{ij}}$, respectively, are

$$r_{Tij} = a_i - e_i x_{ij} \quad \text{and} \quad r_{Rij} = a_i + e_i x_{ij} \quad (4)$$

where $e_i = D/(2a_i)$ means the eccentricity of the i th ellipse and x_{ij} is coordinate of S_{ij} .

But x_{ij} is a function of φ_{Tij} and φ_{Rij} :

$$x_{ij} = r_{Tij} \cos \varphi_{Tij} + \frac{D}{2} \quad \text{and} \quad x_{ij} = r_{Rij} \cos \varphi_{Rij} - \frac{D}{2} \quad (5)$$

Considering that $r_{Tij} + r_{Rij} = 2a_i$ and substituting Eq. (5) to Eq. (4), we can write

$$\frac{1}{1 + e_i \cos \varphi_{Tij}} + \frac{1}{1 - e_i \cos \varphi_{Rij}} = \frac{4a_i}{2a_i - De_i} \quad (6)$$

After transforming Eq. (6), the formula of $\cos \varphi_{Tij}$ versus $\cos \varphi_{Rij}$ has the form [32]:

$$\cos \varphi_{Tij} = \frac{2a_i \cos \varphi_{Rij} + De_i \cos \varphi_{Rij} - 2D}{2a_i + De_i - 2D \cos \varphi_{Rij}} \quad (7)$$

According to the assumptions, the statistical properties of angle of departure (AOD) describe a uniform distribution, i.e., $f_i(\varphi_T) = (2\pi)^{-1}$ for $\varphi_T \in \langle -\pi, \pi \rangle$. Hence, PDF of $\cos \varphi_T$ is

$$f_i(\cos \varphi_T) = f_i(\varphi_T) \left| \frac{d\varphi_T}{d(\cos \varphi_T)} \right| = \frac{1}{2\pi} \frac{1}{\sqrt{1 - \cos^2 \varphi_T}} \quad \text{for } \varphi_T \in \langle -\pi, \pi \rangle \quad (8)$$

Because $\cos \varphi_T$ is a function of $\cos \varphi_R$, so after considering Eq. (7) and Eq. (8), we get [32]:

$$f_i(\cos \varphi_R) = f_i(\cos \varphi_T) \left| \frac{d(\cos \varphi_T)}{d(\cos \varphi_R)} \right| = \frac{1}{2\pi} \frac{1}{|\sin \varphi_R|} \frac{\sqrt{(2a_i + De_i)^2 - 4D^2}}{2a_i + De_i - 2D \cos \varphi_R} \quad \text{for } \varphi_R \in \langle -\pi, \pi \rangle \quad (9)$$

Hence, the demanded form of $f_i(\varphi_R)$ is

$$f_i(\varphi_R) = f_i(\cos \varphi_R) \left| \frac{d(\cos \varphi_R)}{d\varphi_R} \right| = \frac{1}{2\pi} \frac{1 - e_i^2}{1 + e_i^2 - 2e_i \cos \varphi_R} \quad \text{for } \varphi_R \in \langle -\pi, \pi \rangle \quad (10)$$

Eventually, the PDF of AOA for all delayed components, $f_d(\varphi_R)$, takes the form [37]:

$$f_d(\varphi_R) = \sum_{i=1}^N \frac{P_i}{P - P_0} f_i(\varphi_R) = \frac{1}{2\pi} \sum_{i=1}^N \frac{P_i}{P - P_0} \frac{1 - e_i^2}{1 + e_i^2 - 2e_i \cos \varphi_R} \quad \text{for } \varphi_R \in \langle -\pi, \pi \rangle \quad (11)$$

From Eq. (11), it follows that $f_d(\varphi_R)$ depends significantly on P_i and a_i , i.e., on the major axis of each ellipse. This means that properties of this function are determined by the power distribution of the individual time clusters, which is closely related to the transmission properties of a given propagation environment.

3.2. Reception angle dispersion for directional antennas

For directional antennas used in radio links, the evaluation of the reception angle statistical properties is based on simulation tests. In this case, an input data processing algorithm is the basis for the research procedure, which ensures the determining basic parameters and statistical characteristics of AOA. The purpose of simulation studies is to determine a set of pairs (φ_{Rij}, p_{Rij}) that represent the angles and powers of the individual propagation paths reaching the Rx. The analysis of the obtained set is the basis for the assessment of the AOA statistical properties. The relationship between the multi-elliptical structure of the scatterer positions and the environmental transmission characteristics ensures that the simulation results coincide with empirical results.

A procedure scheme of determining φ_{Rij} and p_{Rij} is shown in **Figure 4**.

In the first step of the procedure, the multi-elliptical model parameters are determined based on PDP/PDS. In the next step, the propagation path AODs are generated using the power radiation pattern of the transmitting antenna. For the normalized power pattern, $g_T^2(\varphi_T)$ is

$$\int_{-180^\circ}^{180^\circ} g_T^2(\varphi_T) d\varphi_T = 1 \quad \text{and} \quad g_T^2(\varphi_T) \geq 0 \quad (12)$$

This means that the normalized power radiation pattern meets PDF axioms. Thus, the normalized pattern of the transmitting antenna is used as the PDF of AOD, $f_T(\varphi_T)$:

$$f_T(\varphi_T) = \frac{1}{2\pi} g_T^2(\varphi_T) \quad \text{for} \quad \varphi_T \in \langle -\pi, \pi \rangle \quad (13)$$

For the Gaussian model of the Tx antenna radiation pattern [39]:

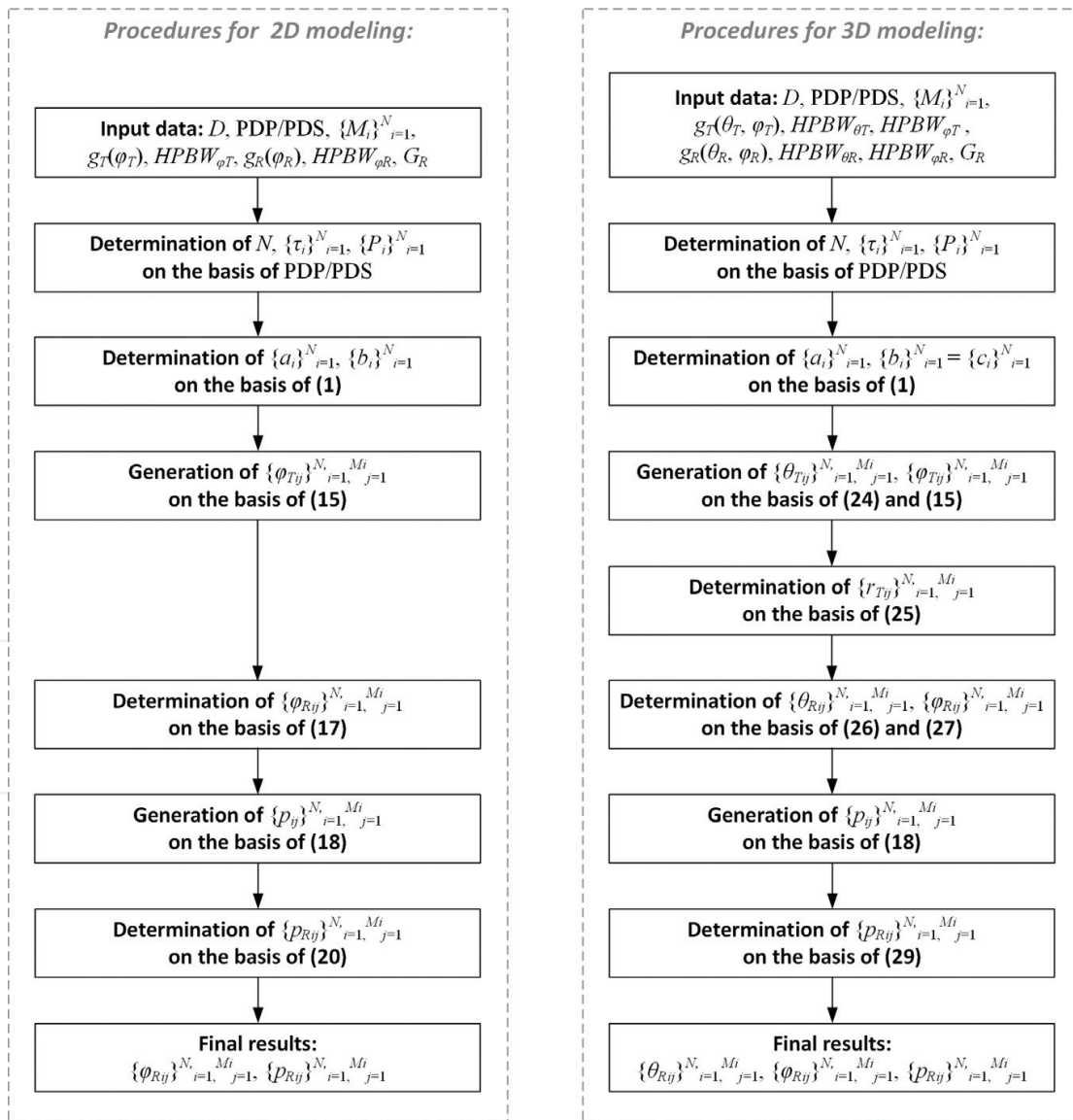


Figure 4. Procedure for determining AOAs and powers of propagation paths for multi-elliptical (2D) and multi-ellipsoidal (3D) propagation model.

$$g_T(\varphi_T) = C_0 \exp\left(-\frac{\varphi_T^2}{2\sigma_{T\varphi}}\right) \quad \text{for } \varphi_T \in \langle -\pi, \pi \rangle, (C_0 - \text{normalizing constant}) \quad (14)$$

we have

$$f_T(\varphi_T) = C_{T\varphi} \exp\left(-\frac{\varphi_T^2}{\sigma_{T\varphi}}\right) \quad \text{for } \varphi_T \in \langle -\pi, \pi \rangle \quad (15)$$

where $C_{T\varphi} = \left(\int_{-180^\circ}^{180^\circ} f_T(\varphi_T) d\varphi_T\right)^{-1} = (\sqrt{\pi}\sigma_{T\varphi} \text{erf}(\pi/\sigma_{T\varphi}))^{-1}$, $\sigma_{T\varphi} = \text{HPBW}_{T\varphi}/(2\sqrt{\ln 2}) \cong 0.6 \text{HPBW}_{T\varphi}$, and $\text{HPBW}_{T\varphi}$ is half power beam width (HPBW) of the transmitting antenna in the azimuth plane.

Eq. (15) is the basis for the AOD generation. A relationship between AOD and AOA results from the ellipse properties [32]:

$$\cos \varphi_{Rij} = \frac{2e_i + (1 + e_i^2) \cos \varphi_{Tij}}{1 + e_i^2 + 2e_i \cos \varphi_{Tij}} \quad (16)$$

Hence [40]:

$$\varphi_{Rij} = \text{sgn}(\varphi_{Tij}) \arccos\left(\frac{2e_i + (1 + e_i^2) \cos \varphi_{Tij}}{1 + e_i^2 + 2e_i \cos \varphi_{Tij}}\right) \quad (17)$$

The j th propagation path of the i th ellipse, i.e., φ_{Rij} , corresponds to the random power, p_{ij} . In the first step, the powers of the delayed components, p_{ij} , are generated based on a uniform distribution:

$$f_p(p_{ij}) = \begin{cases} M_i/(2P_i) & \text{for } p_{ij} \in \langle 0, 2P_i/M_i \rangle \\ 0 & \text{for } p_{ij} \notin \langle 0, 2P_i/M_i \rangle \end{cases} \quad (18)$$

where M_i is the number of the generated paths in the i th cluster, $j = 1, 2, \dots, M_i$, and P_i is the cluster power read from PDP/PDS.

Then, these powers are modified by the power pattern of the receiving antenna, $g_R^2(\varphi_R)$. Let us assume that the main lobe of this pattern is also described using the Gaussian model [39], i.e.,

$$g_R^2(\varphi_R) = G_R \exp\left(-\frac{\varphi_R^2}{\sigma_{R\varphi}}\right) \quad \text{for } \varphi_R \in \langle -\pi, \pi \rangle \quad (19)$$

where G_R is the receiving antenna gain in a linear measure, $\sigma_{R\varphi} = \text{HPBW}_{R\varphi}/(2\sqrt{\ln 2}) \cong 0.6\text{HPBW}_{R\varphi}$, and $\text{HPBW}_{R\varphi}$ is the receiving antenna HPBW in the azimuth plane.

Therefore, p_{ij} generated using by the uniform distribution, i.e., Eq. (18), should be multiplied by the value of the power pattern which corresponds to the AOA with the same indexes, i.e.,

$$p_{Rij} = p_{ij}g_R^2(\varphi_{Rij}) \tag{20}$$

where p_{ij} is the so-called power at the reception point and does not consider the receiving antenna pattern, while p_{Rij} is the power seen at the output of the receiving antenna or at the Rx input [41].

If the receiving antenna is isotropic or omni-directional in the azimuth plane, then it should be assumed that $G_R = 1$ and $g_R^2(\varphi_R) = 1$ for $\varphi_R \in \langle -\pi, \pi \rangle$.

4. Multi-ellipsoidal propagation model

In the case of using antennas, whose pattern width in the vertical plane exceeds several degrees, the scattering in this plane also determines the direction of reaching the propagation paths. Then, we obtain the multi-ellipsoidal propagation model by extending the multi-elliptical model to 3D space. If the antenna heights meet the conditions of $h_T, h_R \ll D$, then this model is reduced to the set of the semi-ellipsoids. As in the case of the multi-elliptical model, the parameters of the individual semi-ellipsoids, i.e., their semi-axes, are defined by Eq. (1) based on PDP/PDS. The reception angle statistical properties are determined based on simulation studies. In this case, we use a procedure for the 3D modeling shown in **Figure 4**. This procedure also includes the elevation plane.

Similar to the multi-elliptical model, the properties of the normalized power radiation pattern of the transmit antenna, $g_T^2(\theta_T, \varphi_T)$, are used to generate AODs [42]:

$$f_T(\theta_T, \varphi_T) = \frac{1}{4\pi}g_T^2(\theta_T, \varphi_T) \sin \theta_T \quad \text{for } \theta_T \in \langle 0, \pi/2 \rangle, \varphi_T \in \langle -\pi, \pi \rangle \tag{21}$$

In this case, we use the assumption of the independence of the scatterer position in the azimuth and elevation planes. Hence, we have

$$f_T(\theta_T, \varphi_T) = f_T(\theta_T) \cdot f_T(\varphi_T) \tag{22}$$

where $f_T(\theta_T)$ and $f_T(\varphi_T)$ are the one-dimensional PDFs of AOD in the elevation and azimuth planes, respectively.

Using the Gaussian model [39] for $g_T(\theta_T, \varphi_T)$, we can describe the PDF of AOD for the multi-ellipsoidal model as

$$f_T(\theta_T, \varphi_T) = f_T(\theta_T) \cdot f_T(\varphi_T) = C_{T\theta} \exp\left(-\frac{(\theta_T - \pi/2)^2}{\sigma_{T\theta}}\right) \sin(\theta_T) \cdot C_{T\varphi} \exp\left(-\frac{\varphi_T^2}{\sigma_{T\varphi}}\right) \tag{23}$$

where $\sigma_{T\theta} = \text{HPBW}_{T\theta} / (2\sqrt{\ln 2}) \cong 0.6\text{HPBW}_{T\theta}$, $\text{HPBW}_{T\theta}$ is the transmitting antenna HPBW in the elevation plane, and $C_{T\theta}$ is a normalizing constant that meets the condition $C_{T\theta} = \left(\int_{0^\circ}^{90^\circ} f_T(\theta_T) d\theta_T \right)^{-1}$.

Thus, $f_T(\varphi_T)$ is described by Eq. (15), while $f_T(\theta_T)$ is defined as

$$f_T(\theta_T) = C_{T\theta} \exp\left(-\frac{(\theta_T - \pi/2)^2}{\sigma_{T\theta}}\right) \sin \theta_T \quad \text{for } \theta_T \in \langle 0, \pi/2 \rangle \quad (24)$$

A generated pair of angles, $(\theta_{Rij}, \varphi_{Rij})$, determines the direction of the ij th propagation path departing from Tx. This path intersects the i th semi-ellipsoid. The intersection point, S_{ij} , determines the potential position of the scatterer. In the multi-ellipsoidal model, the method of determining the distance r_{Tij} between Tx and S_{ij} requires considering the elevation plane. Hence [42]:

$$r_{Tij} = -\frac{1}{2a} b_i^2 D \sin \theta_{Tij} \cos \varphi_{Tij} + \frac{1}{2a} \sqrt{\left(b_i^2 D \sin \theta_{Tij} \cos \varphi_{Tij}\right)^2 + 4ab_i^2 \left(a_i^2 - \frac{D^2}{4}\right)} \geq 0 \quad (25)$$

where $a = \left(b_i \sin \theta_{Tij} \cos \varphi_{Tij}\right)^2 + a_i^2 \left(\cos^2 \theta_{Tij} + \left(\sin \theta_{Tij} \sin \varphi_{Tij}\right)^2\right) \geq 0$.

For the 3D modeling, a pair of angles $(\theta_{Rij}, \varphi_{Rij})$ representing AOA in the elevation and azimuth planes is determined based on the following formula [42]:

$$\theta_{Rij} = \arctan \frac{\sqrt{\left(r_{Tij} \sin \theta_{Tij} \cos \varphi_{Tij} + D\right)^2 + \left(r_{Tij} \sin \theta_{Tij} \sin \varphi_{Tij}\right)^2}}{r_{Tij} \cos \theta_{Tij}} \quad (26)$$

$$\varphi_{Rij} = \text{sgn}(\varphi_{Tij}) \arctan \frac{r_{Tij} \sin \theta_{Tij} \sin \varphi_{Tij}}{r_{Tij} \sin \theta_{Tij} \cos \varphi_{Tij} + D} \quad (27)$$

As in the 2D approach, the random power is assigned to each path that reaches the Rx and is defined by AOA. The procedure for determining this power is analogous to the multi-elliptical model and is based on the uniform distribution and the receiving antenna pattern, $g_R(\theta_R, \varphi_R)$. Let us assume that the main lobe of this pattern is also described using the Gaussian model [39], i.e.,

$$g_R^2(\theta_R, \varphi_R) = G_R \exp\left(-\frac{(\theta_R - \pi/2)^2}{\sigma_{R\theta}}\right) \sin(\theta_R) \cdot \exp\left(-\frac{\varphi_R^2}{\sigma_{R\varphi}}\right) \quad \text{for } \theta_R \in \langle 0, \pi/2 \rangle, \varphi_R \in \langle -\pi, \pi \rangle \quad (28)$$

where $\sigma_{R\theta} = \text{HPBW}_{R\theta} / (2\sqrt{\ln 2}) \cong 0.6\text{HPBW}_{R\theta}$ and $\text{HPBW}_{R\theta}$ the receiving antenna HPBW in the elevation plane.

Then, p_{ij} generated using the uniform distribution, i.e., Eq. (18), should be multiplied by the value of the pattern corresponding to the elevation and azimuth angles of the same indexes. Hence

$$p_{Rij} = p_{ij} g_R^2(\theta_{Rij}, \varphi_{Rij}) \quad (29)$$

For an isotropic receiving antenna, we accept $G_R = 1$ and $g_R^2(\theta_R, \varphi_R) = 1$ for $\theta_T \in \langle 0, \pi/2 \rangle$, and $\varphi_R \in \langle -\pi, \pi \rangle$.

5. Reception angle distribution for local scattering components

Modeling the reception angle statistical properties for the local scattering components is based on the von Mises distribution [1, 4]:

$$f_0(\varphi_R) = \frac{\exp(\gamma_\varphi \cos \varphi_R)}{2\pi I_0(\gamma_\varphi)} \quad \text{for } \varphi_R \in \langle -\pi, \pi \rangle \quad (30)$$

where $I_0(\cdot)$ is the zero-order modified Bessel function and $\gamma_\varphi \geq 0$ is a parameter describing the reception angle dispersion in the azimuth plane.

For the 3D case, considering the independence of the scatterer occurrence in the azimuth and elevation planes, we have [42]:

$$f_0(\theta_R, \varphi_R) = f_0(\theta_R) \cdot f_0(\varphi_R) = C_{M\theta} \frac{\exp\left(\gamma_\theta \cos\left(\frac{\pi}{2} - \theta_R\right)\right)}{2\pi I_0(\gamma_\theta)} \cdot \frac{\exp(\gamma_\varphi \cos \varphi_R)}{2\pi I_0(\gamma_\varphi)} \quad (31)$$

for $\theta_R \in \langle 0, \pi/2 \rangle, \varphi_R \in \langle -\pi, \pi \rangle$

where $C_{M\theta} = \left(\int_{0^\circ}^{90^\circ} f_0(\theta_R) d\theta_R\right)^{-1} = 2\pi I_0(\gamma_\theta) \left(\int_{0^\circ}^{90^\circ} \exp\left(\gamma_\theta \cos\left(\frac{\pi}{2} - \theta_R\right)\right) d\theta_R\right)^{-1}$ and $\gamma_\theta \geq 0$ is a parameter determining the angle dispersion in the elevation plane.

The values of γ_φ and γ_θ depend on surroundings of the receiving antenna in an analyzed propagation scenario.

For $\gamma_\varphi = \{0, 3, 30\}$, PDFs of AOA for the local scattering components in the azimuth plane are shown in **Figure 5**.

It should be noted that the AOA distribution for the local scattering components is independent of the distance between Tx and Rx, D . This PDF depends only on the obstacles in the

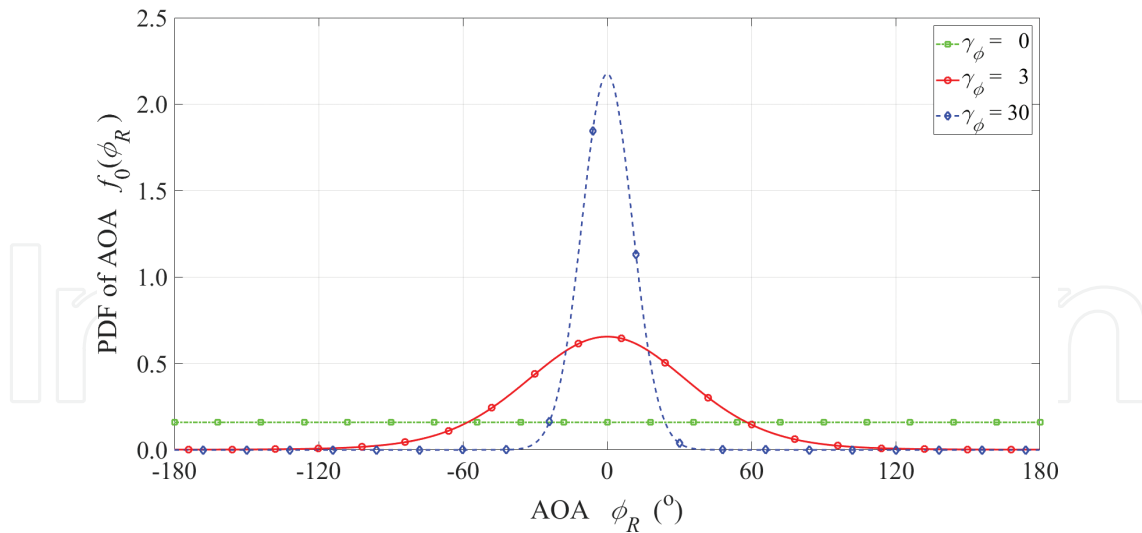


Figure 5. PDFs of AOA for local scattering components and selected γ_ϕ .

immediate vicinity of Rx and the direction of Rx-Tx. For the local scattering components, the random power can also be assigned to each AOA. The generation method of such power is similar to that for the delayed scattering components. However, the power at the reception point, p_{0j} , is determined on the basis of another uniform distribution [42]:

$$f_p(p_{0j}) = \begin{cases} (\kappa + 1)M_0/(2P_0) & \text{for } p_{0j} \in \langle 0, 2P_0/(M_0(\kappa + 1)) \rangle \\ 0 & \text{for } p_{0j} \notin \langle 0, 2P_0/(M_0(\kappa + 1)) \rangle \end{cases} \quad (32)$$

where M_0 is the number of the generated paths, $j = 1, 2, \dots, M_0$, and P_0 is the value of power read from PDP/PDS for $\tau \cong 0$.

The power at the Rx input, p_{R0j} , is determined as for the delayed scattering components, based on Eq. (20) or Eq. (28) for the 2D or 3D modeling, respectively.

6. Sample results of simulation studies

6.1. Influence of antenna parameters on reception angle distribution

A result of simulation studies is sets of the propagation path parameters reaching the Rx. In the multi-elliptical model, input data for the analysis of the result PDF of AOA for the delayed and local scattering components are two sets $\Phi = \{\varphi_{Rij}\}$ and $\mathbf{P} = \{p_{Rij}\}$ for $j = 1, 2, \dots, M_i$ and $i = 0, 1, \dots, N$. For the multi-ellipsoidal model, a set of elevations is additionally considered, i.e., $\Theta = \{\theta_{Rij}\}$. Thus, the ij th propagation path is defined by two or three parameters, for 2D or 3D modeling, respectively. The method of determining the estimated PDFs of AOA based on these sets is presented in [41, 42].

Let $\mathbf{O}(\theta_R, \varphi_R) = \{(i, j) : \theta_{Rij} \in (\theta_R \pm \varepsilon_\theta) \wedge \varphi_{Rij} \in (\varphi_R \pm \varepsilon_\varphi)\}$, where ε_θ and ε_φ are the neighborhoods of θ_R and φ_R , respectively. Thus, $\sum_{\mathbf{O}(\theta_R, \varphi_R)} p_{Rij}(\theta_{Rij}, \varphi_{Rij})$ represents the total power of the signal that arrives at the input of the receiver from $(\theta_R \pm \varepsilon_\theta, \varphi_R \pm \varepsilon_\varphi)$ sector.

An estimator of a joint PDF of AOA for the delayed and local scattering components is defined as [41]:

$$\tilde{f}_R(\theta_R, \varphi_R) = C_0 \frac{\sum_{\mathbf{O}(\theta_R, \varphi_R)} p_{Rij}(\theta_{Rij}, \varphi_{Rij})}{\sum_{i=0}^N \sum_{j=1}^{M_i} p_{Rij}(\theta_{Rij}, \varphi_{Rij})} \quad (33)$$

where C_0 is a normalizing constant that is associated with ε_θ and ε_φ and provides a condition

$$\lim_{\substack{\varepsilon_\theta \rightarrow 0 \\ \varepsilon_\varphi \rightarrow 0}} \int_0^{90^\circ} \int_{-180^\circ}^{180^\circ} \tilde{f}_R(\theta_R, \varphi_R) d\theta_R d\varphi_R = 1.$$

Eq. (33) is the basis for determining PDFs of AOA in the elevation and azimuth planes. In this case, marginal distribution properties are applied.

Thus, the PDFs of AOA in the elevation and azimuth planes have forms, respectively [41]:

$$\tilde{f}_R(\theta_R) = C_{R\theta} \frac{\sum_{i=0}^N p_{Rij}(\theta_{Rij})}{\sum_{i=0}^N \sum_{j=1}^{M_i} p_{Rij}(\theta_{Rij})} \quad \text{and} \quad \tilde{f}_R(\varphi_R) = C_{R\varphi} \frac{\sum_{i=0}^N p_{Rij}(\varphi_{Rij})}{\sum_{i=0}^N \sum_{j=1}^{M_i} p_{Rij}(\varphi_{Rij})} \quad (34)$$

where $\mathbf{K}(\theta_R) = \{(i, j) : \theta_{Rij} \in (\theta_R \pm \varepsilon_\theta)\}$ and $\mathbf{L}(\varphi_R) = \{(i, j) : \varphi_{Rij} \in (\varphi_R \pm \varepsilon_\varphi)\}$, whereas $C_{R\theta}$

and $C_{R\varphi}$ meet conditions $\lim_{\varepsilon_\theta \rightarrow 0} \int_0^{90^\circ} \tilde{f}_R(\theta_R) d\theta_R = 1$ and $\lim_{\varepsilon_\varphi \rightarrow 0} \int_{-180^\circ}^{180^\circ} \tilde{f}_R(\varphi_R) d\varphi_R = 1$, respectively.

For the simulation results presented below, we adopted the following assumptions: the PDP as shown in **Figure 2**, carrier frequency, $f_0 = 2.4$ GHz, $D = 300$ m, and parameters for four antenna types [43]:

- “Corner reflector” (CR): $G_{R-CR} = 23$ dBi, $HPBW_{\theta-CR} = 18^\circ$, and $HPBW_{\varphi-CR} = 58^\circ$
- “Horn antenna” (HA): $G_{R-HA} = 23$ dBi, $HPBW_{\theta-HA} = 40^\circ$, and $HPBW_{\varphi-HA} = 44^\circ$
- “Parabolic grid” (PG): $G_{R-PG} = 46$ dBi, $HPBW_{\theta-PG} = 14^\circ$, and $HPBW_{\varphi-PG} = 10^\circ$
- “Other antenna” (OA): $G_{R-OA} = 23$ dBi and $HPBW_{\theta-OA} = 6^\circ$ and $HPBW_{\varphi-OA} \rightarrow 360^\circ$

Figure 6 shows examples of the PDFs of AOA in the elevation and azimuth planes for the CR-transmitting antenna and OA-receiving antenna. The individual PDFs are presented for selected α_T . Whereas, the exemplary marginal PDFs of AOA for the CR receiving antenna and OA transmitting antenna are shown in **Figure 7**. In this case, the PDFs are depicted for selected α_R . These graphs show an influence of the directional antenna on the angular dispersion at the transmitting and receiving side, respectively.

The marginal PDFs of AOA for four types of antennas—CR, HA, PG, and OA—are shown in **Figure 8**. In this case, we assume that $\alpha_T = 180^\circ$, $\alpha_R = 0$, and the radiation patterns of the transmitting and receiving antennas are the same.

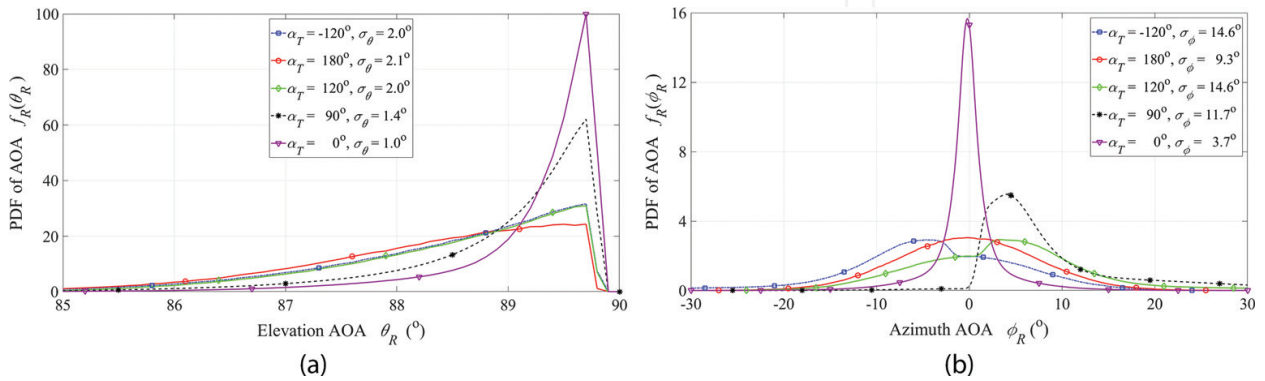


Figure 6. PDFs of AOA in (a) elevation and (b) azimuth planes for selected α_T .

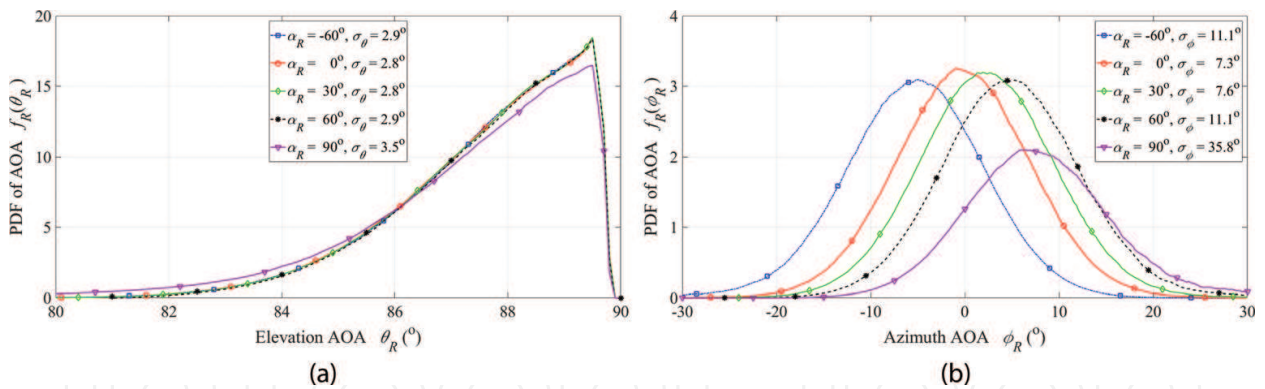


Figure 7. PDFs of AOA in (a) elevation and (b) azimuth planes for selected α_R .

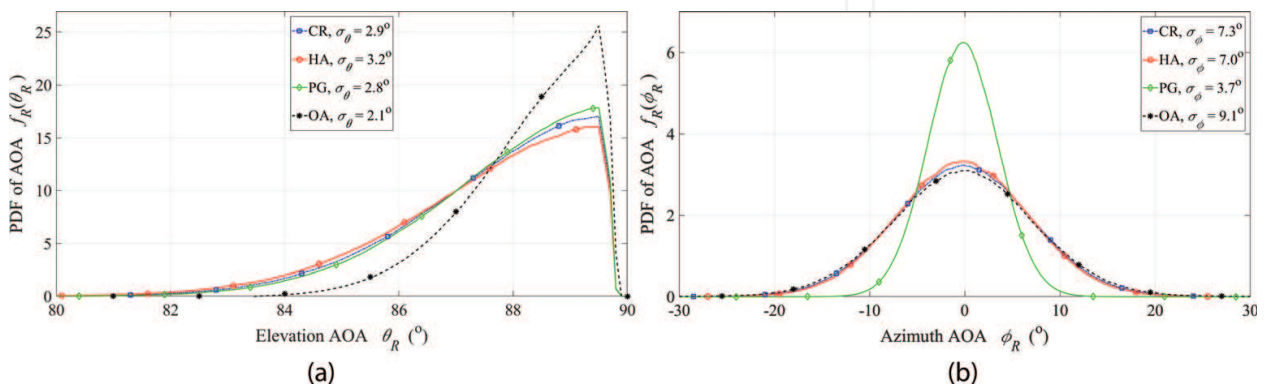


Figure 8. PDFs of AOA in (a) elevation and (b) azimuth planes for four antenna types.

The PDFs are the basis for assessing the AOA dispersion for different types of propagation environments. A quantitative evaluation of the dispersion is based on the rms angle spread (AS). This measure is defined in the elevation, σ_θ , and azimuth, σ_φ , planes, respectively [39]:

$$\sigma_\theta = \sqrt{\int_0^{90^\circ} \theta_R^2 \cdot f_R(\theta_R) d\theta_R - \left(\int_0^{90^\circ} \theta_R \cdot f_R(\theta_R) d\theta_R \right)^2} \quad (35)$$

$$\sigma_\varphi = \sqrt{\int_{-180^\circ}^{180^\circ} \varphi_R^2 \cdot f_R(\varphi_R) d\varphi_R - \left(\int_{-180^\circ}^{180^\circ} \varphi_R \cdot f_R(\varphi_R) d\varphi_R \right)^2} \quad (36)$$

Figure 9 shows the relationship between AS and $HPBW_{T\theta} = HPBW_{R\theta}$ for $HPBW_{T\varphi} = HPBW_{R\varphi}$ equal to $HPBW_{\varphi-CR} = 58^\circ$ or $HPBW_{\varphi-PG} = 10^\circ$. ASs versus $HPBW_{T\varphi} = HPBW_{R\varphi}$ for $HPBW_{T\theta} = HPBW_{R\theta}$ equal to $HPBW_{\theta-CR} = 18^\circ$ or $HPBW_{\theta-HA} = 40^\circ$ is presented in **Figure 10**.

In both cases, we assume that the Tx and Rx antennas are oriented toward each other.

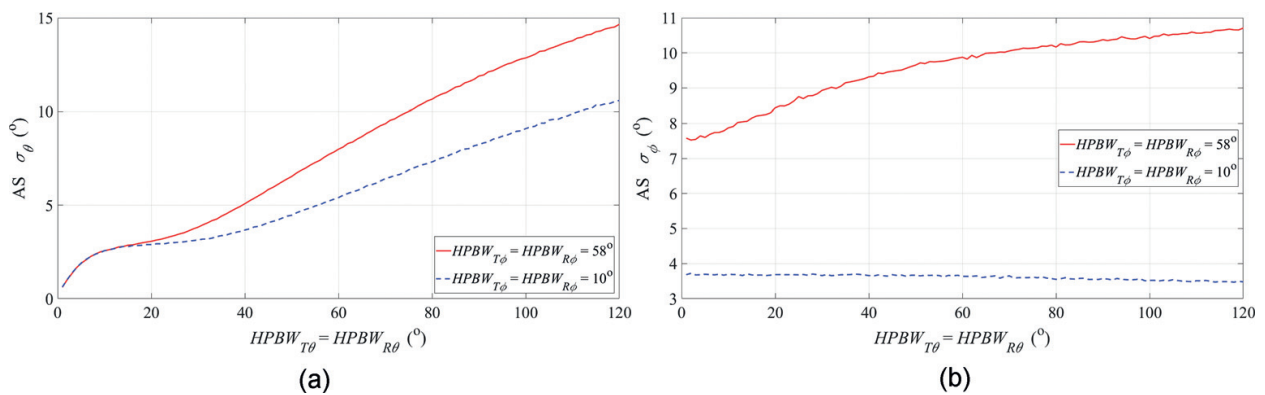


Figure 9. ASs in (a) elevation and (b) azimuth planes versus $HPBW_{T\theta} = HPBW_{R\theta}$ for $HPBW_{T\varphi} = HPBW_{R\varphi}$ equal $HPBW_{\varphi-CR} = 58^\circ$ or $HPBW_{\varphi-PG} = 10^\circ$.

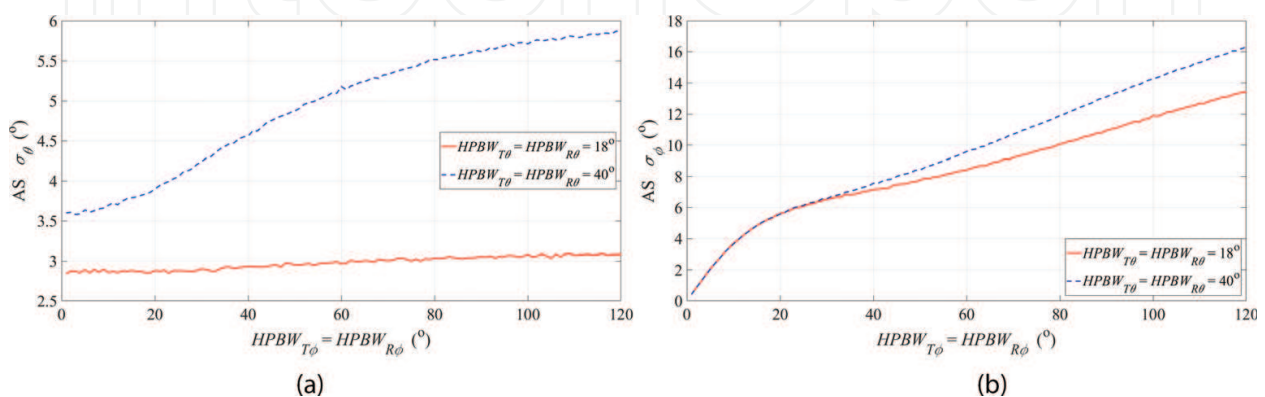


Figure 10. ASs in (a) elevation and (b) azimuth planes versus $HPBW_{T\varphi} = HPBW_{R\varphi}$ for $HPBW_{T\theta} = HPBW_{R\theta}$ equal $HPBW_{\theta-CR} = 18^\circ$ or $HPBW_{\theta-HA} = 40^\circ$.

An influence of the radiation/reception direction of the transmitting/receiving antenna on the AS is illustrated in **Figures 11** and **12** for (variable α_T , $\alpha_R = 0 = \text{const.}$) and ($\alpha_T = 180^\circ = \text{const.}$, variable α_R), respectively. These graphs are obtained for four analyzed antenna types.

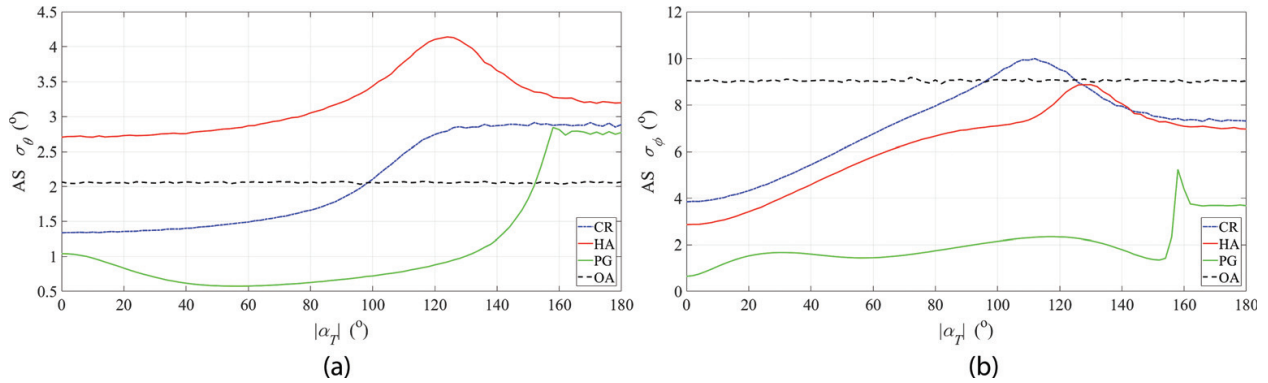


Figure 11. ASs in (a) elevation and (b) azimuth planes versus α_T .

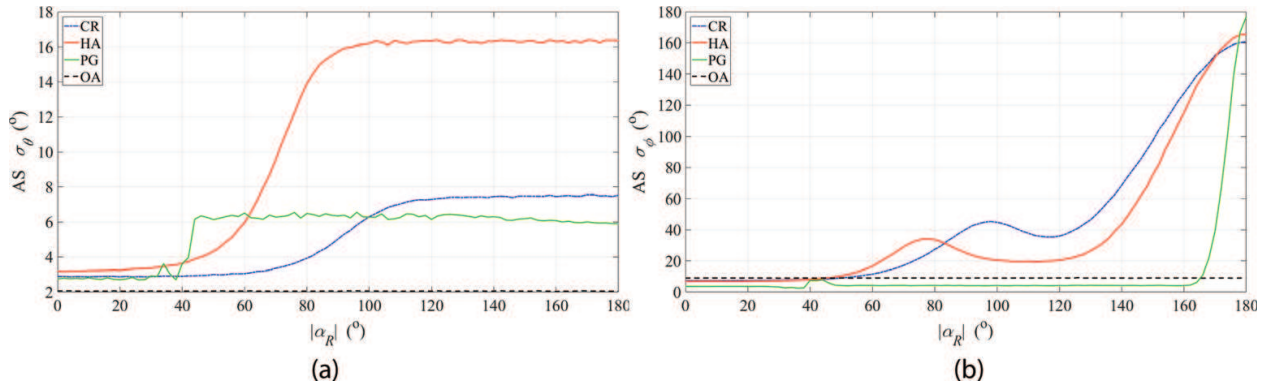


Figure 12. ASs in (a) elevation and (b) azimuth planes versus α_R .

As a result of scattering phenomenon, the minimum AS occurs when the transmitting antenna radiates in the opposite direction to the Rx location. However, it should be remembered that in this case, the total power of the delayed components is reduced.

The results presented in this chapter are obtained for 2.4 GHz frequency. The evaluation of the AOA statistical properties for other frequency ranges is presented in [32, 37, 40, 42] for 1.8 GHz and in [41] for 28 GHz. The results presented in the chapter and these papers concern the angular distribution. As is shown in ([33], **Figure 8**) and ([2], **Figure 1**), AS is strictly linear correlated with the rms delay spread. Whereas, from ([7], Table 7.7.3-2), we see that the delay spread is reduced with the frequency increase. Therefore, we can conclude that the increase in the frequency brings the decrease in the angular dispersion.

6.2. Effects of reception angle dispersion on correlational and spectral properties

Multipath propagation and channel dispersion phenomena as well as an object motion effect have a significant impact on deformation of spectral and correlational structures of the

transmitted signals. Therefore, the assessment of the environment impact on the correlation-spectral properties requires an accurate mapping of these phenomena. For this purpose, we propose the so-called Doppler multi-elliptical channel model (DMCM), which is depicted in [44]. This model describes a procedure for generating the propagation path parameters in simulation studies. In addition to the angular dispersion, DMCM also considers the movement of the objects (Tx/Rx). Obtained simulation results using DMCM give the opportunity to evaluate instantaneous or statistical (averaged) changes of the received signal properties. Additionally in [44], DMCM is verified on the basis of empirical data available in a literature.

The influence analysis of the angular dispersion in DMCM on the correlational and spectral properties is presented in [45, 46]. In this case, the impact of the Rx motion direction on an autocorrelation function (ACF), power density spectrum (PSD), and following parameters—a coherence time, average Doppler frequency, Doppler spread, and asymmetry coefficient—is analyzed.

The basis for assessing the angular dispersion effects on the ACF and PSD is the relationship between the Doppler frequency shift (DFS) and AOA. DFS representing the ij th propagation path is determined based on the following formula:

$$f_{Dij} = f_{Dmax} \cos(\varphi_{Rij} - \beta) \tag{37}$$

where $f_{Dmax} = f_0 v/c$ is the maximum DFS, f_0 is carrier frequency of the transmitting signal, v is Rx velocity, and β is Rx movement direction in relation to the Rx-Tx direction.

Typical assumptions are adopted in the presented analysis. The unmodulated carrier wave signal is used to assess the angular dispersion effects on the correlational and spectral properties. This approach gives an opportunity to simplify an analytical description and provides partial verification and comparison of obtained results with others presented in a literature. In this case, the PSD analyzed in a baseband is called the Doppler spectrum. In addition, the uniform distribution of phase and independence of the signal components are accepted.

Then, an ACF estimator is defined as [47]:

$$\tilde{R}(\tau) = \sum_{i=0}^N \sum_{j=1}^{M_i} p_{Rij} \exp(i2\pi f_{Dij} \tau) \tag{38}$$

The PSD is obtained based on the Wiener-Khinchin theorem [48, 49]:

$$S(f_D) = \int_{-\infty}^{\infty} R(\tau) \exp(-i2\pi f_D \tau) d\tau \tag{39}$$

To this aim, we use the fast Fourier transform algorithm and smoothing filtering.

An unequivocal assessment of the influence of spatial parameters on the transmission properties of an environment requires normalization of ACF and PSD. Therefore, the results obtained

in the simulation studies are normalized with respect to the average power, $R_x(0)$, of the received signal. So, for the ACF and PSD, we have, respectively [45]:

$$r(\tau) = \frac{R(\tau)}{R(0)} \quad \text{and} \quad s(f_D) = 2f_{D\max} \frac{S(f_D)}{R(0)} \quad (40)$$

Based on these definitions, the properties of the normalized ACF and PSD are $r(0) = 1$ and

$$\frac{1}{2f_{D\max}} \int_{-f_{D\max}}^{f_{D\max}} s(f_D) df_D = 1.$$

In the assessment of the AOA dispersion effects on the correlational and spectral properties, a spatial scenario presented in **Figure 13** is analyzed.

In this case, we assume that the Rx moves along a straight road at a constant speed, $v = 50\text{ km/h}$. The distance from the route to the Tx is $D_y = 500\text{ m}$. The Tx emits the harmonic signal at $f_0 = 2.4\text{ GHz}$, so $f_{D\max} \cong 111\text{ Hz}$. The antenna patterns are omni-directional. The ACF and PSD evaluations are carried out at four points of the Rx route for specific directions: (A) $\beta = 30^\circ$, (B) $\beta = 60^\circ$, (C) $\beta = 90^\circ$, and (D) $\beta = 120^\circ$. For four analyzed cases, modules of the normalized ACFs and PSDs are presented in **Figure 14**.

A quantitative assessment of the channel dispersion impact on the spectral and correlational properties can be based on the parameter analysis. For the ACF, the coherence time, T_C , is determined based on the following condition:

$$|r(T_C)| = \left| \frac{R(T_C)}{R(0)} \right| = \frac{1}{2} \quad (41)$$

However, for the PSD, the average DFS, F_D , rms Doppler spread, σ_D , and asymmetry coefficient, μ_D , [50] are defined, respectively:

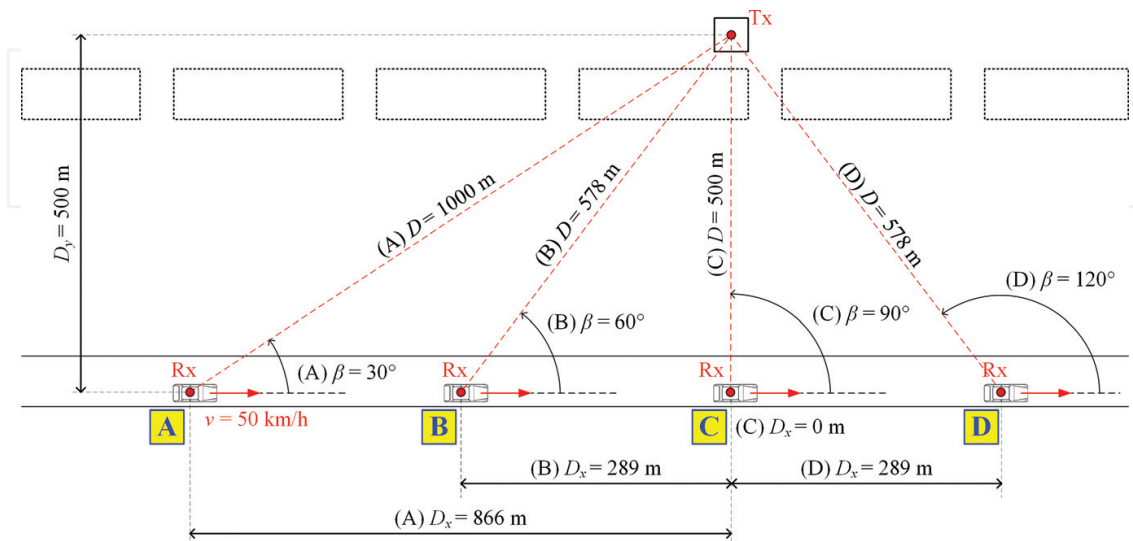


Figure 13. Spatial scenario of simulation studies.

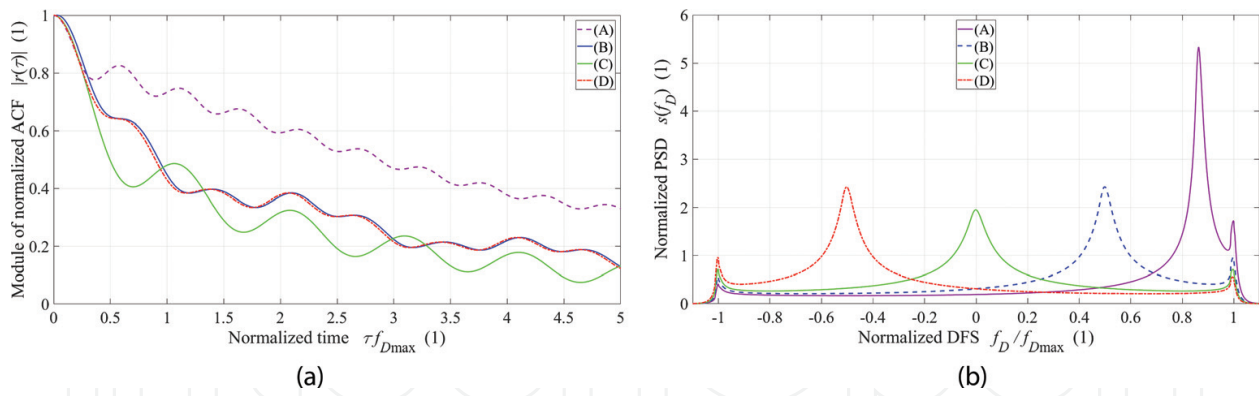


Figure 14. Module of normalized ACFs and PSDs for four analyzed points along Rx route.

$$F_D = 2f_{Dmax} \int_{-f_{Dmax}}^{f_{Dmax}} f_D s(f_D) df_D \quad (42)$$

$$\sigma_D = \sqrt{2f_{Dmax} \int_{-f_{Dmax}}^{f_{Dmax}} (f_D - F_D)^2 s(f_D) df_D} \quad (43)$$

$$\mu_D = \frac{1}{\sqrt{\sigma_D}} \sqrt[3]{2f_{Dmax} \int_{-f_{Dmax}}^{f_{Dmax}} (f_D - F_D)^3 s(f_D) df_D} \quad (44)$$

To obtain independence of the above metrics from f_{Dmax} , i.e., from f_0 and v , we introduce normalized parameters in the following forms: $T_C f_{Dmax}$, F_D/f_{Dmax} , σ_D/f_{Dmax} , and μ_D . Changes of these parameters on the analyzed route are shown in Figure 15.

A characteristic feature of the presented PSD graphs is an occurrence of maxima for extreme DFSs and DFS resulted from Eq. (37) for the direct path component. The last frequency is closely related to the angle, β , between the velocity vector and the Rx-Tx direction. Based on the obtained results presented in Figures 14 and 15, we can conclude that close relations exist between the parameters of the analyzed characteristics and the spatial parameters of the simulation scenario. We can conclude that T_C , σ_D , $|F_D|$, and $|\mu_D|$ are decreasing with reduction of the Rx-Tx distance. The results prove that PSDs and ACFs significantly depend not only on the time domain dispersion but also on the angular dispersion and mutual position of the Rx and Tx. A graphical illustration of this fact is shown in Figure 16, which shows the PSD changes versus the Rx position.

Based on Figure 16, it follows that channels in mobile radiocommunications are spatially anisotropic due to their correlation-spectral properties. This means that the analysis of the ACF and PSD requires not only knowledge of the transmission properties of an environment but also knowledge about the Rx-Tx mutual position and movement parameters of the

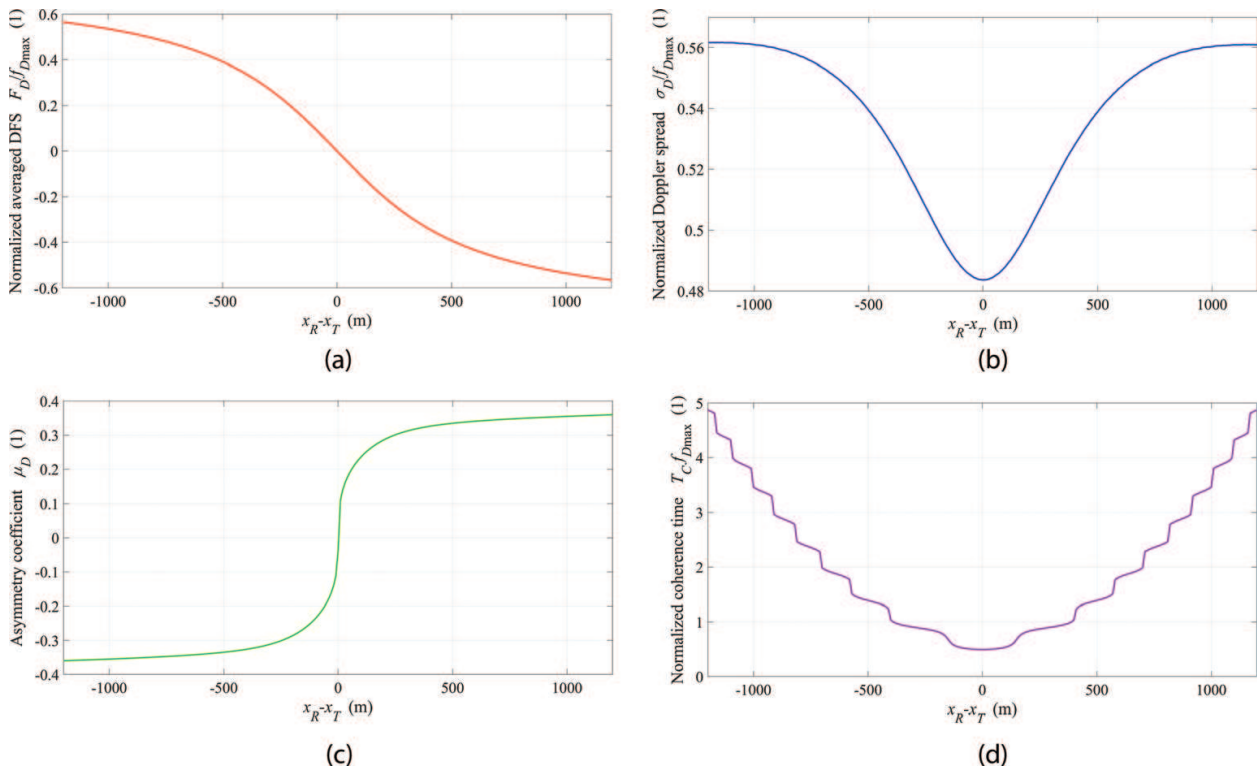


Figure 15. Changes of normalized parameters on Rx route: (a) average Doppler, (b) Doppler spread, (c) asymmetry coefficient, and (d) coherence time.

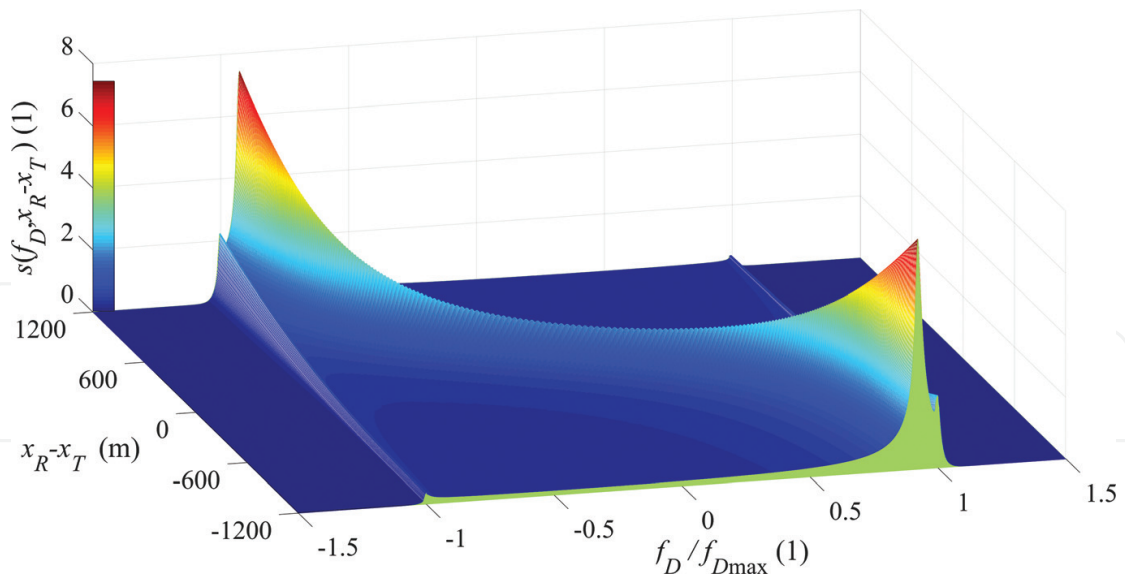


Figure 16. Averaged PSD versus Rx position.

elements of communication system. It follows that the set of parameters qualifying correctness of the PSD and ACF analysis, in addition to the characteristics related to the channel impulse response (PDP/PDS), should include the Tx and Rx positions, spatial location of movement trajectory, direction, and value of the velocity vector of the moving object. Therefore, the

channel transmission characteristics (PDP/PDS) condition the nature of the angular dispersion of the received signal in multipath propagation environments.

7. Conclusion

The chapter is devoted to the problem of the multipath propagation phenomenon modeling and its impact on changes of the received signal properties. The main focus is on the method of determining the PDF of AOA, which has the significant impact on changes in the correlational and spectral properties. In contrast to the empirical models, using the geometry-based models gives the opportunity to consider in the modeling process the spatial structure of a propagation environment. Linking the environment transmission properties with the position geometry of the scatterers is the main problem of using the geometric models. The use of the multi-elliptical or multi-ellipsoidal models is a solution to this problem. In this case, the geometrical structure of the scatterer locations in the form of the set of the confocal ellipses or semi-ellipsoids is created on the basis of the transmission characteristics of a propagation environment. This ensures adapting the geometrical structure to the analyzed or modeled propagation environment. The use of the multi-ellipsoidal or multi-elliptical models gives the possibility to consider the effect of the antenna radiation patterns on the PDF of AOA. This plays a significant role in the analysis of the compatible operating of coexistent wireless systems. PDF of AOA is the basis for assessing the impact of a propagation environment on the correlational and spectral properties of the transmitted signals. The use of the geometric models presented in this chapter provides mapping of the motion effects, which cause changes in the ACFs and PSDs versus changes of the object positions. The ability to adapt to the environment transmission properties and the assessment of changes in the correlation-spectral characteristics as a function of the object locations significantly distinguishes the models described in this chapter, among those presented so far in a literature.

Author details

Jan M. Kelner* and Cezary Ziólkowski

*Address all correspondence to: jan.kelner@wat.edu.pl

Military University of Technology, Faculty of Electronics, Institute of Telecommunications, Warsaw, Poland

References

- [1] Ziólkowski C, Kelner JM. Empirical models of the azimuthal reception angle—Part I: Comparative analysis of empirical models for different propagation environments. *Wireless Personal Communications*. 2016;**91**(2):771-791. DOI: 10.1007/s11277-016-3496-1

- [2] Ziółkowski C, Kelner JM. Empirical models of the azimuthal reception angle—Part II: Adaptation of the empirical models in analytical and simulation studies. *Wireless Personal Communications*. 2016;**91**(3):1285-1296. DOI: 10.1007/s11277-016-3528-x
- [3] Sieskul BT, Kupferschmidt C, Kaiser T. Spatial fading correlation for local scattering: A condition of angular distribution. *IEEE Transactions on Vehicular Technology*. 2011;**60**(3): 1271-1278. DOI: 10.1109/TVT.2010.2103370
- [4] Abdi A, Barger JA, Kaveh M. A parametric model for the distribution of the angle of arrival and the associated correlation function and power spectrum at the mobile station. *IEEE Transactions on Vehicular Technology*. 2002;**51**(3):425-434. DOI: 10.1109/TVT.2002.1002493
- [5] WINNER II Channel Models. IST-WINNER II. Tech. Rep. Deliverable 1.1.2 v.1.2. 2007
- [6] 3GPP TR 25.996 v13.1.0 (2016-12). Spatial Channel Model for Multiple Input Multiple Output (MIMO) Simulations (Release 13). Tech. Rep. 3GPP TR 25.996 v13.1.0. Valbonne, France. 3rd Generation Partnership Project (3GPP), Technical Specification Group Radio Access Network; 2016
- [7] 3GPP TR 38.901 V14.2.0 (2017-09). Study on channel model for frequencies from 0.5 to 100 GHz (Release 14). Tech. Rep. 3GPP TR 38.901 V14.2.0. Valbonne, France. 3rd Generation Partnership Project (3GPP), Technical Specification Group Radio Access Network; 2017
- [8] Yun Z, Iskander MF. Ray tracing for radio propagation modeling: Principles and applications. *IEEE Access*. 2015;**3**:1089-1100. DOI: 10.1109/ACCESS.2015.2453991
- [9] Fuschini F, Vitucci EM, Barbiroli M, Falciasacca G, Degli-Esposti V. Ray tracing propagation modeling for future small-cell and indoor applications: A review of current techniques. *Radio Science*. 2015;**50**(6):2015RS005659. DOI: 10.1002/2015RS005659
- [10] Corucci A, Usai P, Monorchio A, Manara G. Wireless propagation modeling by using ray-tracing. In: Mittra R. editor. *Computational Electromagnetics. Recent Advances and Engineering Applications*. New York, NY, USA: Springer; 2014. pp. 575-618. DOI: 10.1007/978-1-4614-4382-7_17
- [11] Lim SY, Yun Z, Iskander MF. Radio propagation modeling: A unified view of the ray-tracing image method across emerging indoor and outdoor environments. In: Lakhtakia A, Furse CM, editors. *The World of Applied Electromagnetics. In Appreciation of Magdy Fahmy Iskander*. Cham, Switzerland: Springer; 2018. pp. 301-328. DOI: 10.1007/978-3-319-58403-4_13
- [12] Yun Z, Iskander MF. Radio propagation modeling and simulation using ray tracing. In: Lakhtakia A, Furse CM, editors. *The World of Applied Electromagnetics. In Appreciation of Magdy Fahmy Iskander*. Cham, Switzerland: Springer; 2018. pp. 275-299. DOI: 10.1007/978-3-319-58403-4_12
- [13] Lee WCY. Estimate of local average power of a mobile radio signal. *IEEE Transactions on Vehicular Technology*. 1985;**34**(1):22-27. DOI: 10.1109/T-VT.1985.24030

- [14] Janaswamy R. Angle and time of arrival statistics for the Gaussian scatter density model. *IEEE Transactions on Wireless Communications*. 2002;**1**(3):488-497. DOI: 10.1109/TWC.2002.800547
- [15] Jiang L, Tan SY. Geometrically Based Statistical Channel Models for Outdoor and Indoor Propagation Environments. *IEEE Transactions on Vehicular Technology*. 2007;**56**(6):3587-3593. DOI: 10.1109/TVT.2007.901055
- [16] Le KN. On angle-of-arrival and time-of-arrival statistics of geometric scattering channels. *IEEE Transactions on Vehicular Technology*. 2009;**58**(8):4257-4264. DOI: 10.1109/TVT.2009.2023255
- [17] Olenko AY, Wong KT, EH-O N. Analytically derived TOA-DOA statistics of uplink/downlink wireless multipaths arisen from scatterers on a hollow-disc around the mobile. *IEEE Antennas and Wireless Propagation Letters*. 2003;**2**(1):345-348. DOI: 10.1109/LAWP.2004.824174
- [18] Baltzis KB. A generalized elliptical scattering model for the spatial characteristics of mobile channels. *Wireless Personal Communications*. 2011;**67**(4):971-984. DOI: 10.1007/s11277-011-0434-0
- [19] Zhang J, Pan C, Pei F, Liu G, Cheng X. Three-dimensional fading channel models: A survey of elevation angle research. *IEEE Communications Magazine*. 2014;**52**(6):218-226. DOI: 10.1109/MCOM.2014.6829967
- [20] Janaswamy R. Angle of arrival statistics for a 3-D spheroid model. *IEEE Transactions on Vehicular Technology*. 2002;**51**(5):1242-1247. DOI: 10.1109/TVT.2002.801756
- [21] Olenko AY, Wong KT, Qasmi SA, Ahmadi-Shokouh J. Analytically derived uplink/downlink TOA and 2-D-DOA distributions with scatterers in a 3-D hemispheroid surrounding the mobile. *IEEE Transactions on Antennas and Propagation*. 2006;**54**(9):2446-2454. DOI: 10.1109/TAP.2006.880661
- [22] Nawaz SJ, Khan NM, Patwary MN, Moniri M. Effect of directional antenna on the Doppler spectrum in 3-D mobile radio propagation environment. *IEEE Transactions on Vehicular Technology*. 2011;**60**(7):2895-2903. DOI: 10.1109/TVT.2011.2161788
- [23] Nawaz SJ, Riaz M, Khan NM, Wyne S. Temporal analysis of a 3D ellipsoid channel model for the vehicle-to-vehicle communication environments. *Wireless Personal Communications*. 2015;**82**(3):1337-1350. DOI: 10.1007/s11277-015-2286-5
- [24] Zajic AG, Stüber GL. Three-dimensional modeling, simulation, and capacity analysis of space-time correlated mobile-to-mobile channels. *IEEE Transactions on Vehicular Technology*. 2008;**57**(4):2042-2054. DOI: 10.1109/TVT.2007.912150
- [25] Olenko AY, Wong KT, Qasmi SA. Distribution of the uplink multipaths' arrival delay and azimuth-elevation arrival angle because of 'bad urban' scatterers distributed cylindrically above the mobile. *Transactions on Emerging Telecommunications Technologies*. 2013;**24**(2):113-132. DOI: 10.1002/ett.2530

- [26] Ahmed A, Nawaz SJ, Gulfam SM. A 3-D propagation model for emerging land mobile radio cellular environments. *PLoS One*. 2015;**10**(8):e0132555. DOI: 10.1371/journal.pone.0132555
- [27] Nawaz SJ, Wyne S, Baltzis KB, Gulfam SM, Cumanan K. A tunable 3-D statistical channel model for spatio-temporal characteristics of wireless communication networks. *Transactions on Emerging Telecommunications Technologies*. 2017;**28**(12):e3213. DOI: 10.1002/ett.3213
- [28] Jiang L, Tan SY. Simple geometrical-based AOA model for mobile communication systems. *Electronics Letters*. 2004;**40**(19):1203-1205. DOI: 10.1049/el:20045599
- [29] Petrus P, Reed JH, Rappaport TS. Geometrical-based statistical macrocell channel model for mobile environments. *IEEE Transactions on Communications*. 2002;**50**(3):495-502. DOI: 10.1109/26.990911
- [30] Ertel RB, Reed JH. Angle and time of arrival statistics for circular and elliptical scattering models. *IEEE Journal on Selected Areas in Communications*. 1999;**17**(11):1829-1840. DOI: 10.1109/49.806814
- [31] Khan NM, Simsim MT, Rapajic PB. A generalized model for the spatial characteristics of the cellular mobile channel. *IEEE Transactions on Vehicular Technology*. 2008;**57**(1):22-37. DOI: 10.1109/TVT.2007.904532
- [32] Ziółkowski C. Statistical model of the angular power distribution for wireless multipath environments. *IET Microwaves, Antennas & Propagation*. 2015;**9**(3):281-289. DOI: 10.1049/iet-map.2014.0099
- [33] Pedersen KI, Mogensen PE, Fleury BH. A stochastic model of the temporal and azimuthal dispersion seen at the base station in outdoor propagation environments. *IEEE Transactions on Vehicular Technology*. 2000;**49**(2):437-447. DOI: 10.1109/25.832975
- [34] Pedersen KI, Mogensen PE, Fleury BH. Spatial channel characteristics in outdoor environments and their impact on BS antenna system performance. In: *Proceedings of the 1998 48th IEEE Vehicular Technology Conference (VTC)*; 18-21 May 1998; Ottawa, Canada: IEEE; 1998. vol. 2; p. 719-723. DOI: 10.1109/VETEC.1998.683676
- [35] Mogensen PE, Pedersen KI, Leth-Espensen P, Fleury BH, Frederiksen F, Olesen K, Larsen SL. Preliminary measurement results from an adaptive antenna array testbed for GSM/UMTS. In: *Proceedings of the 1997 47th IEEE Vehicular Technology Conference (VTC)*; 4-7 May 1997; Phoenix, AZ, USA: IEEE; 1997. vol. 3; p. 1592-1596. DOI: 10.1109/VETEC.1997.605826
- [36] Fleury BH, Tschudin M, Heddergott R, Dahlhaus D, Pedersen KI. Channel parameter estimation in mobile radio environments using the SAGE algorithm. *IEEE Journal on Selected Areas in Communications*. 1999;**17**(3):434-450. DOI: 10.1109/49.753729
- [37] Ziółkowski C, Kelner JM. Estimation of the reception angle distribution based on the power delay spectrum or profile. *International Journal of Antennas and Propagation*. 2015;**2015**:e936406. DOI: 10.1155/2015/936406

- [38] Parsons JD, Bajwa AS. Wideband characterisation of fading mobile radio channels. IEE Proceedings F Communications, Radar and Signal Processing. 1982;**129**(2):95-101. DOI: 10.1049/ip-f-1:19820016
- [39] Vaughan R, Bach Andersen J. Channels, Propagation and Antennas for Mobile Communications. London, UK: Institution of Engineering and Technology; 2003
- [40] Ziółkowski C, Kelner JM, Nowosielski L, Wnuk M. Modeling the distribution of the arrival angle based on transmitter antenna pattern. In: Proceedings of the 2017 11th European Conference on Antennas and Propagation (EUCAP); 19-24 March 2017; Paris, France: IEEE; 2017. p. 1582-1586. DOI: 10.23919/EuCAP.2017.7928823
- [41] Ziółkowski C, Kelner JM. Statistical evaluation of the azimuth and elevation angles seen at the output of the receiving antenna. IEEE Transactions on Antennas and Propagation. 2018;**66**. DOI: 10.1109/TAP.2018.2796719
- [42] Ziółkowski C, Kelner JM. Antenna pattern in three-dimensional modelling of the arrival angle in simulation studies of wireless channels. IET Microwaves, Antennas & Propagation. 2017;**11**(6):898-906. DOI: 10.1049/iet-map.2016.0591
- [43] Azevedo JA, Santos FE, Sousa TA, Agrela JM. Impact of the antenna directivity on path loss for different propagation environments. IET Microwaves, Antennas & Propagation. 2015;**9**(13):1392-1398. DOI: 10.1049/iet-map.2015.0194
- [44] Ziółkowski C, Kelner JM. Geometry-based statistical model for the temporal, spectral, and spatial characteristics of the land mobile channel. Wireless Personal Communications. 2015;**83**(1):631-652. DOI: 10.1007/s11277-015-2413-3
- [45] Ziółkowski C, Kelner JM. Influence of receiver/transmitter motion direction on the correlational and spectral signal properties. In: Proceedings of the 2016 10th European Conference on Antennas and Propagation (EuCAP); 10-15 April 2016; Davos, Switzerland: IEEE; 2016. pp. 1-4. DOI: 10.1109/EuCAP.2016.7481225
- [46] Kelner JM, Ziółkowski C. Influence of receiver/transmitter motion direction on the correlational and spectral characteristics – Simulation analysis. In: Proceedings of the 2016 10th International Conference on Signal Processing and Communication Systems (ICSPCS); 19-21 December 2016; Gold Coast, Australia: IEEE; 2016. p. 1-6. DOI: 10.1109/ICSPCS.2016.7843381
- [47] Stüber GL. Principles of Mobile Communication. 3rd ed. New York, NY, USA: Springer; 2011
- [48] Wiener N. Generalized harmonic analysis. Acta Math. 1930;**55**(1):117-258. DOI: 10.1007/BF02546511
- [49] Khintchine AY. Korrelationstheorie der stationären stochastischen Prozesse. Mathematische Annalen. 1934;**109**(1):604-615. DOI: 10.1007/BF01449156
- [50] Beckmann P. Probability in Communication Engineering. New York, NY, USA: Harcourt, Brace & World; 1967

